Instability towards Staggered Loop Currents in the Three-Orbital Model for Cuprate Superconductors

S. Bulut and A. P. Kampf
Theoretical Physics III, Center for Electronic Correlations and Magnetism, Institute of Physics, University of Augsburg, 86135 Augsburg, Germany

W. A. Atkinson
Department of Physics and Astronomy, Trent University, Peterborough Ontario, Canada, K9J7B8

(Dated: November 23, 2015)

We present evidence for the existence of a spontaneous instability towards an orbital loop-current phase in a multiorbital Hubbard model for the CuO_2 planes in cuprates. Contrary to the previously proposed θ_{II} phase with intra-unit cell currents, the identified instability is towards a staggered pattern of intertwined current loops. The orbitally resolved current pattern thereby shares its staggered character with the proposal of d-density wave order. The current pattern will cause a Fermi surface reconstruction and the opening of a pseudogap. We argue that the pseudogap phase with time-reversal symmetry breaking currents is susceptible to further phase transitions and therefore offers a route to account for axial incommensurate charge order and a polar Kerr effect in underdoped cuprates.

I. INTRODUCTION

There is now considerable evidence in underdoped cuprate high-temperature superconductors for a cascade of phase transitions, starting at high temperatures with the pseudogap onset at T^*, followed by incommensurate charge order (ICO) at $T_{\rm co} < T^*$ and superconductivity at $T_c < T_{\rm co}$. In addition, broken time-reversal symmetry has been associated with T^* and a Kerr rotation is measured below a temperature $T_{\rm Kerr}$ with $T_{\rm Kerr} \sim 0.75T^*$ over wide doping range. At present, there is no unifying theory that explains this intriguing sequence of transitions.

Ultrasound spectroscopy suggests that T^* corresponds to a true thermodynamic phase transition[1] ; this finding challenges the viewpoint that the pseudogap arises as a correlation induced phenomenon in a symmetry unbroken paramagnetic phase. Below T^* spin-polarized neutron scattering experiments detected weak magnetic moments[2–5]. These moments appear to preserve the translational symmetry of the lattice, and led to the proposal of intra-unit cell loop currents (LCs)[6]. However, the so-called θ_{II} LC phase by itself has difficulty explaining the partial gapping of charge excitations[7]. While variational methods favored the existence of LC phases in finite clusters[8,9], alternative numerically exact analyses reported no evidence for the θ_{II} phase[10,11].

The Kerr effect[12,13] that sets in below $T_{\rm Kerr}$ is further evidence for time-reversal symmetry breaking, but also requires that mirror symmetries be broken[14]. Throughout much of the cuprate phase diagram, $T_{\rm Kerr}$ and $T_{\rm co}$[15–23] are close, which has motivated further proposals in which fluctuating charge-[14,24] or pair-density wave states[25,26] generate spontaneous current patterns with broken mirror symmetries. These scenarios assume a heirarchy of transitions associated with distinct symmetry breakings needed to form the fully ordered density-wave state. Other proposals follow the common theme that the pseudogap results from the competition between two or more order parameters[27–30].

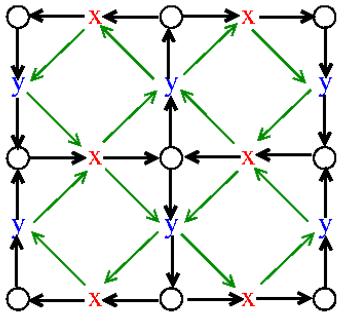

FIG. 1: (Color online) Staggered pattern of spontaneous loop currents. Open circle,"x" and "y" symbols denote Cu$d_{x^2-y^2}$, Op_x and Op_y orbitals, respectively. Currents along p-d bonds (black arrows) are about three times stronger than those in p-p bonds (green arrows).

The ICO phase involves predominantly a charge transfer between oxygen orbitals in the CuO_2 planes[20–22,31,32]. This challenges notions of immutable CuO_2 bands, and points to the necessity to employ multiorbital models for the ICO phase[33–35]. Here, we support this reasoning and show that orbital resolved intra-unit cell physics is important throughout the pseudogap regime.

In this work we report the results of an unbiased calculation for a three-band model of CuO_2 planes which verifies the existence of an instability towards a staggered pattern of intertwined LCs (Fig. 1). This "πLC" phase is different from the anticipated θ_{II} phase, but shares its ordering wavevector $\mathbf{Q} = (\pi, \pi)$ with the earlier phenomenological proposal of LCs in the d-density wave (DDW) state[36,37]. In the πLC phase the Fermi surface reconstructs to form hole pockets with a concomitant pseudogap-like structure in the electronic spectrum. For realistic parameters, the ICO reported previously for

the same model Hamiltonian[34] is subleading to the πLC instability. Yet, the presence of staggered order favors a subsequent instability towards ICO with axial wavevectors connecting the tips of the hole pockets[35], consistent with experiments. The charge modulation of the latter necessarily breaks mirror symmetries and will hence allow for a polar Kerr signal[14]. This scenario is offered as a proposal for the cascade of phase transitions in the pseudogap regime of underdoped cuprates.

II. HAMILTONIAN

The unit cell of a single CuO_2 plane is shown in Fig. 2, along with the choice of orbital phases and the corresponding signs of the hopping terms.

The non-interacting part of the three band model is given by

$$\hat{H}_0 = \sum_{i\alpha\sigma} \epsilon_{i\alpha} \hat{n}_{i\alpha\sigma} + \sum_{i\alpha j\beta\sigma} t_{i\alpha j\beta} \hat{c}^\dagger_{i\alpha\sigma} \hat{c}_{j\beta\sigma} \tag{1}$$

where i and j are unit cell labels, α and β are orbital labels, σ is the spin label, $\epsilon_{i\alpha}$ is the orbital energy, $\hat{n}_{i\alpha\sigma}$ is the number operator, $t_{i\alpha j\beta}$ is the tunneling matrix element between orbital $i\alpha$ and $j\beta$, and $\hat{c}_{i\alpha\sigma}$ and $\hat{c}^\dagger_{i\alpha\sigma}$ are annihilation and creation operators. Below, we suppress the spin labels.

Using the translational invariance, $\hat{H}_0$ can be Fourier transformed to reciprocal space:

$$\hat{H}_0 = \sum_{\mathbf{k}} \Psi^\dagger_{\mathbf{k}} \mathbf{H}_0(\mathbf{k}) \Psi_{\mathbf{k}} \tag{2}$$

where $\Psi^\dagger_{\mathbf{k}} = [\hat{c}^\dagger_{\mathbf{k}d}, \hat{c}^\dagger_{\mathbf{k}x}, \hat{c}^\dagger_{\mathbf{k}y}]$, and $\hat{c}^\dagger_{\mathbf{k}\alpha}$ ($\hat{c}_{\mathbf{k}\alpha}$) is the creation (annihilation) operator for an electron with crystal momentum $\mathbf{k}$ and orbital α. Explicitly,

$$\hat{c}_{\mathbf{k}\alpha} = \frac{1}{\sqrt{N}} \sum_i e^{-i\mathbf{k}\cdot\mathbf{R}_{i\alpha}} \hat{c}_{i\alpha} \tag{3}$$

$$\hat{c}^\dagger_{\mathbf{k}\alpha} = \frac{1}{\sqrt{N}} \sum_i e^{i\mathbf{k}\cdot\mathbf{R}_{i\alpha}} \hat{c}^\dagger_{i\alpha} \tag{4}$$

where N is the number of unit cells in the system, and $\mathbf{R}_{i\alpha}$ is the position vector of α'th orbital in i'th unit cell. $H_0(\mathbf{k})$ is readily obtained by plugging Eqs. (3) and (4) into Eq. (1):

$$\mathbf{H}_0(\mathbf{k}) = \begin{pmatrix} \epsilon_d & -2it_{pd}s_x & 2it_{pd}s_y \\ 2it_{pd}s_x & \epsilon_x & 4t_{pp}s_x s_y \\ -2it_{pd} & 4t_{pp}s_x s_y & \epsilon_y \end{pmatrix} \tag{5}$$

where $s_x = \sin(k_x/2)$ and $s_y = \sin(k_y/2)$. A more convenient form of $\mathbf{H}_0$ is obtained after the following gauge transformation:

$$\hat{c}_{\mathbf{k}x} \rightarrow i\hat{c}_{\mathbf{k}x} \tag{6}$$

$$\hat{c}^\dagger_{\mathbf{k}x} \rightarrow -i\hat{c}^\dagger_{\mathbf{k}x} \tag{7}$$

$$\hat{c}_{\mathbf{k}y} \rightarrow i\hat{c}_{\mathbf{k}y} \tag{8}$$

$$\hat{c}^\dagger_{\mathbf{k}y} \rightarrow -i\hat{c}_{\mathbf{k}y}. \tag{9}$$

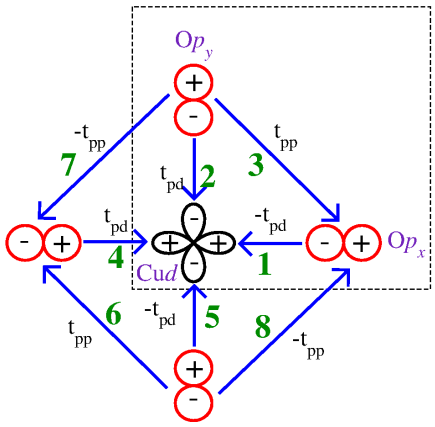

FIG. 2: (Color online) Unit cell of a CuO_2 plane (dashed box). The orbital phase convention is indicated by the sign of the hopping matrix elements. Numbers in green enumerate the inequivalent bonds, and the direction of the blue arrows indicates a positive sign of the current flow for the current operator definitions given in Appendix A.

Hence, the final form of $\mathbf{H}_0$ is obtained:

$$\mathbf{H}_0(\mathbf{k}) = \begin{pmatrix} \epsilon_d & 2t_{pd}s_x & -2t_{pd}s_y \\ 2t_{pd}s_x & \epsilon_p & 4t_{pp}s_x s_y \\ -2t_{pd}s_y & 4t_{pp}s_x s_y & \epsilon_p \end{pmatrix}. \tag{10}$$

We set $t_{pd} = 1$ so that it defines the unit of energy.

The interacting part of the Hamiltonian includes the intra- (U_α) and inter-orbital ($V_{i\alpha,j\beta}$) Coulomb interactions

$$\hat{H}' = \sum_{i\alpha\sigma, j\beta\sigma'} \left[\delta_{i\alpha,j\beta}(1-\delta_{\sigma,\sigma'})U_\alpha + \frac{V_{i\alpha,j\beta}}{2} \right] \hat{n}_{i\alpha\sigma}\hat{n}_{j\beta\sigma'}, \tag{11}$$

where i, j are unit cell indices, α, β are orbital labels and $V_{i\alpha,j\beta}$ is nonzero for nearest-neighbors only. Throughout, we suppress the spin index σ, set $t_{pp} = -0.5$, $\epsilon_d - \epsilon_p = 2.5$, $U_d = 9$, $U_p = 3$, $V_{pd} = 2.2$, and $V_{pp} = 1$ unless otherwise stated. The Hamiltonian $\hat{H} = \hat{H}_0 + \hat{H}'$ is thus the conventional three-band model of cuprates[38] with a typical parameter set[39].

III. INTERACTING CURRENT SUSCEPTIBILITY

The current operator associated with the bond between sites $i\alpha$ and $j\beta$ is $\hat{J}_{i\alpha,j\beta} = -it_{i\alpha,j\beta}(\hat{c}^\dagger_{i\alpha}c_{j\beta} - \hat{c}^\dagger_{j\beta}\hat{c}_{i\alpha})$ where $t_{i\alpha,j\beta}$ is the corresponding hopping matrix element. If $\langle \hat{J}_{i\alpha,j\beta} \rangle > 0$ then current flows from $j\beta$ to $i\alpha$. In momentum space, the current operator along bond m is given by

$$\hat{J}_m(\mathbf{q}) = -i \sum_{\mathbf{k}} [h^m_{\alpha\beta}(\mathbf{k},\mathbf{q})\hat{c}^\dagger_{\mathbf{k}\alpha}\hat{c}_{\mathbf{k}+\mathbf{q}\beta} - h^m_{\beta\alpha}(\mathbf{k},\mathbf{q})\hat{c}^\dagger_{\mathbf{k}\beta}\hat{c}_{\mathbf{k}+\mathbf{q}\alpha}] \tag{12}$$

where α, β are the orbitals associated with the bond and the matrix elements of the current operators $h^m_{\alpha\beta}(\mathbf{k},\mathbf{q})$ are listed in Table I. As shown in Fig. 2, there are eight distinct bonds on the CuO_2 lattice. Accordingly the current susceptibility,

$$\chi^J_{mn}(\mathbf{q}, i\omega_\ell) = \int_0^\beta d\tau\, e^{i\omega_\ell \tau} \langle \hat{J}_m(\mathbf{q},\tau)\hat{J}_n(-\mathbf{q},0)\rangle, \quad (13)$$

is an 8×8 matrix, where $\omega_\ell = 2\pi\ell T$ denotes the bosonic Matsubara frequencies. Each matrix element can be decomposed as

$$\chi^J_{mn} = \chi^{mn}_{\alpha\beta\alpha'\beta'} - \chi^{mn}_{\alpha\beta\beta'\alpha'} - \chi^{mn}_{\beta\alpha\alpha'\beta'} + \chi^{mn}_{\beta\alpha\beta'\alpha'} \quad (14)$$

where

$$\begin{aligned}\chi^{mn}_{\theta\theta'\gamma\gamma'}(\mathbf{q}, i\omega_\ell) &= \frac{-1}{N}\sum_{\mathbf{k}\mathbf{k}'} h^m_{\theta\theta'}(\mathbf{k},\mathbf{q}) h^n_{\gamma\gamma'}(\mathbf{k}',-\mathbf{q}) \\ &\times \int_0^\beta d\tau\, e^{i\omega_\ell\tau}\langle \hat{c}^\dagger_{\mathbf{k}\theta}(\tau) c_{\mathbf{k}+\mathbf{q}\theta'}(\tau) \\ &\times \hat{c}^\dagger_{\mathbf{k}'\gamma}(0) c_{\mathbf{k}'-\mathbf{q}\gamma'}(0)\rangle. \quad (15)\end{aligned}$$

Previously, we investigated charge instabilities in the same three-band model with non-local interactions using a generalized random phase approximation (gRPA)[34,40]. While methods like QMC or cluster DMFT are at first glance more desirable as they are designed to handle strong local correlations, they are less accurate in treating non-local interactions, and are also limited in momentum-space resolution. Although it neglects strong correlation physics, the gRPA has the advantage that it treats local and non-local interactions on the same footing, and is unbiased with respect to wavevector and to the unit cell-resolved current pattern. Within gRPA, the 2-particle vertex function includes both exchange and direct interaction diagrams and hence also generates combinations of both (see Fig. 3), while Green functions remain unrenormalized.

Following Ref.[34], we project the interactions onto a set of 19 basis functions $g^i_{\alpha\beta}(\mathbf{k})$ in orbital and momentum space, leading to a 19×19 matrix equation for the effective interaction vertex $\tilde{\Gamma}^{ij}(q)$, where $q \equiv (\mathbf{q}, \omega)$, and i, j label the basis functions. The basis functions and the interaction vertex are the same as in Ref.[34]. Closing $\tilde{\Gamma}^{ij}(q)$ on the left and right with current vertex functions $A^{i,\eta m}_{\alpha\alpha'}(q)$ yields the susceptibility

$$\chi^{mn}_{\alpha\alpha'\beta\beta'}(q) = \chi^{0,mn}_{\alpha\alpha'\beta\beta'}(q) - \sum_{ij} A^{i,Lm}_{\alpha\alpha'}(q)\tilde{\Gamma}^{ij}(q) A^{j,Rn}_{\beta\beta'}(q), \quad (16)$$

where

$$\begin{aligned}\chi^{0,\ell_1\ell_2}_{\alpha\alpha'\beta\beta'}(q) &= \frac{1}{N}\sum_{\mathbf{k}\mu\nu} h^{\ell_1}_{\alpha\alpha'}(\mathbf{k},\mathbf{q}) M^{\alpha'\beta\beta'\alpha}_{\mu\nu\mathbf{k}q} F^{\nu\mu}_{\mathbf{k}\mathbf{q}}(\omega) h^{\ell_2}_{\beta\beta'}(\mathbf{k}-\mathbf{q},\mathbf{q}), \\ A^{i,L\ell}_{\alpha\alpha'} &= \frac{1}{N}\sum_{\mathbf{k}\mu\nu\theta\theta'} h^\ell_{\alpha\alpha'}(\mathbf{k},\mathbf{q}) M^{\alpha'\theta\theta'\alpha}_{\mu\nu\mathbf{k}q} F^{\nu\mu}_{\mathbf{k}\mathbf{q}}(\omega) g^i_{\theta\theta'}(\mathbf{k}) \quad (17) \\ A^{i,R\ell}_{\alpha\alpha'} &= \frac{1}{N}\sum_{\mathbf{k}\mu\nu\theta\theta'} h^\ell_{\alpha\alpha'}(\mathbf{k}-\mathbf{q},\mathbf{q}) M^{\alpha'\theta\theta'\alpha}_{\mu\nu\mathbf{k}q} F^{\nu\mu}_{\mathbf{k}\mathbf{q}}(\omega) g^i_{\theta\theta'}(\mathbf{k}) \\ M^{\gamma'\theta\theta'\gamma}_{\mu\nu\mathbf{k}q} &= S_{\gamma'\nu}(\mathbf{k}) S^*_{\theta\nu}(\mathbf{k}) S_{\theta'\mu}(\mathbf{k}+\mathbf{q}) S^*_{\gamma\mu}(\mathbf{k}+\mathbf{q}) \quad (18) \\ F^{\nu\mu}_{\mathbf{k}\mathbf{q}}(\omega) &= \frac{f(E^\nu_{\mathbf{k}}) - f(E^\mu_{\mathbf{k}+\mathbf{q}})}{\omega + E^\nu_{\mathbf{k}} - E^\mu_{\mathbf{k}+\mathbf{q}} + i\delta}, \quad (19)\end{aligned}$$

ℓ denotes bond indices, $h^\ell_{\alpha\alpha'}(\mathbf{k},\mathbf{q})$ are matrix elements of the current operators which are explicitly defined in Table I, $S_{\alpha\nu}(\mathbf{k})$ is the αth element of the νth eigenvector of $\mathbf{H}_0(\mathbf{k})$, $S^*_{\alpha\nu}(\mathbf{k})$ is its complex conjugate, $E^\nu_{\mathbf{k}}$ are the eigenvalues, $f(E)$ is the Fermi function, and i and δ in Eq. 19 are the complex constant and a small broadening parameter respectively. The bare current susceptibility $\chi^{0,mn}_{\alpha\alpha'\beta\beta'}(q)$ and the functions $A^{i,L\ell}_{\alpha\alpha'}(q)$ and $A^{i,R\ell}_{\alpha\alpha'}(q)$ differ from Ref.[34] as they contain current operators.

ℓ	$\theta\theta'$	$h^\ell_{\theta\theta'}(\mathbf{k},\mathbf{q})$
1	dx	$t_{pd}e^{i(q_x+k_x)/2}$
1	xd	$-t_{pd}e^{-ik_x/2}$
2	dy	$-t_{pd}e^{i(q_y+k_y)/2}$
2	yd	$t_{pd}e^{-ik_y/2}$
3	xy	$-it_{pp}e^{i(q_y-k_x+k_y)/2}$
3	yx	$-it_{pp}e^{i(q_x+k_x-k_y)/2}$
4	dx	$-t_{pd}e^{-i(q_x+k_x)/2}$
4	xd	$t_{pd}e^{ik_x/2}$
5	dy	$t_{pd}e^{-i(q_y+k_y)/2}$
5	yd	$-t_{pd}e^{ik_y/2}$
6	xy	$-it_{pp}e^{-i(q_y+k_x-k_y)/2}$
6	yx	$-it_{pp}e^{-i(q_x+k_x-k_y)/2}$
7	xy	$it_{pp}e^{i(q_y+k_x+k_y)/2}$
7	yx	$it_{pp}e^{-i(q_x+k_x+k_y)/2}$
8	xy	$it_{pp}e^{-i(q_y+k_x+k_y)/2}$
8	yx	$it_{pp}e^{i(q_x+k_x+k_y)/2}$

TABLE I: Matrix elements of the current operator. i is the imaginary constant. The overall sign of each term results from three factors: the complex constant in the current operator definitions, the sign of the hopping terms, and the gauge transformation.

We search for the existence of spontaneous currents by following the evolution of the current susceptibility upon cooling. The instability is signalled by a divergence of the momentum-resolved susceptibility at zero frequency $\chi^J_{mn}(\mathbf{q}, \omega = 0)$.

IV. RESULTS

Figure 4 shows typical results for the current susceptibility. The inset shows that the matrix element $\chi^J_{11}(\mathbf{q}, \omega = 0)$, corresponding to currents along the d-p_x bonds, becomes strongly peaked at $\mathbf{q} = \mathbf{Q} \equiv (\pi, \pi)$ as the temperature is lowered. This peak indeed diverges upon cooling to the critical temperature near $T = 0.01$ (main

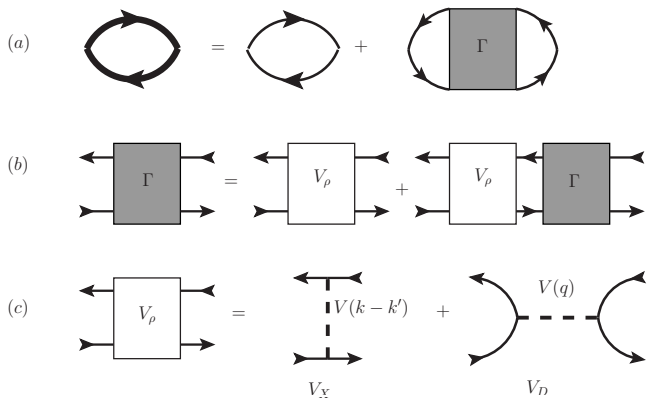

FIG. 3: Diagrammatic structure of gRPA: (a) Interacting susceptibility, (b) vertex function, (c) effective interaction. Reprinted with permission from[34]. ©American Physical Society.

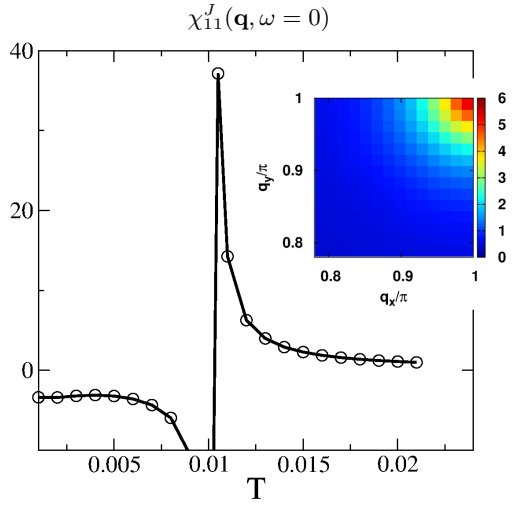

FIG. 4: (Color online) Temperature evolution of $\chi^J_{11}(\mathbf{Q},\omega=0)$ for $\mathbf{Q}=(\pi,\pi)$. (inset) $\chi^J_{11}(\mathbf{q},\omega=0)$ at $T=0.011$. The parameter values are $V_{pd}=2.2$, $V_{pp}=1$, and the hole density is $p=0.13$.

panel), which signals an instability towards a current-carrying state. The ordering wavevector $\mathbf{Q}$ of the πLC phase is the same as in the DDW scenario,[36] and should be contrasted with the θ_{II} phase,[6] for which $\mathbf{q}=\mathbf{0}$.

The example result in Fig. 4 was obtained for $V_{pd}=2.2$ and $V_{pp}=1$. However, the instability towards a πLC phase persists when $V_{pp}=0$, and hence is driven by the Coulomb repulsion V_{pd} between copper and oxygen orbitals. In fact, also the local interactions U_d and U_p have no effect on the πLC instability. As we have explicitly verified, the staggered current instability originates from the exchange (ladder only) diagrams.

As previously established[35], an ICO with a predominant charge redistribution between Op_x and Op_y orbitals can be generated by the Coulomb repulsion V_{pp} between Op_x and Op_y orbitals. Based on the inter-orbital distances, we expect $V_{pd}>V_{pp}$, which implies that loop currents emerge at higher temperatures than ICO. Indeed, for our parameter values, the critical temperature for the πLC instability is about twice as large as the critical temperature for ICO.

To determine the bond-resolved πLC pattern, we calculate the eigenvector of the leading eigenvalue of the current susceptibility matrix. In the current operator basis $\hat{J}_1(\mathbf{q}),\ldots,\hat{J}_8(\mathbf{q})$, this normalized eigenvector is $[0.48,-0.48,-0.15,0.48,-0.48,-0.15,-0.15,-0.15]$; this eigenvector reveals the direction and the relative magnitudes of the currents on the eight inequivalent bonds: all bonds are involved in the πLC instability, and for the selected parameter set the currents along the p-d bonds are about three times stronger than those along the p-p bonds. The relative strength of the p-d and p-p currents varies with the ratio t_{pp}/t_{pd}. The wavevector $\mathbf{Q}$ of the instability further implies that the pattern alternates between adjacent unit cells. We thus obtain the cartoon shown in Fig. 1, in which two distinct (green and black) and interpenetrating loop currents are evident. This pattern is similar to the previously proposed current-carrying phases of either the DDW -[36] or the staggered flux-phase type[41–43], but differs in having two circulating current loops one of which involves oxygen orbitals only.

The instability towards spontaneous πLCs will naturally reconstruct the Fermi surface. To explore this we implement the πLCs on the mean-field level. The starting point for this calculation is the general identity $\hat{n}_a\hat{n}_b=(\hat{J}_{ab}\hat{J}^*_{ab}/t^2_{ab}+\hat{n}_a+\hat{n}_b)/2$ that is true for any pair of orbitals a and b[44]. Hence, the non-local density-density interactions $\frac{1}{2}\sum_{i\alpha,j\beta}V_{i\alpha,j\beta}\hat{n}_{i\alpha}\hat{n}_{j\beta}$ can be decoupled by introducing the current amplitudes $z_{i\alpha,j\beta}=\langle\hat{J}_{i\alpha,j\beta}\rangle=\pm z_{\alpha\beta}$. The mean-field version of the interorbital Coulomb interactions thus reads:

$$\hat{H}'_{MF}=\tilde{\epsilon}_p(\hat{n}_x+\hat{n}_y)+\tilde{\epsilon}_d\hat{n}_d-\sum_{\langle i\alpha,j\beta\rangle}\frac{V_{i\alpha,j\beta}}{2t^2_{i\alpha,j\beta}}\hat{J}_{i\alpha,j\beta}z_{i\alpha,j\beta} \tag{20}$$

where $\tilde{\epsilon}_p=V_{pd}+2V_{pp}$ and $\tilde{\epsilon}_d=2V_{pd}$ renormalize the orbital energies. The intraorbital interactions lead to additional Hartree shifts of the orbital energies; these are assumed to be already included in ϵ_d and ϵ_p. We obtain the mean field Hamiltonian $\hat{H}_{MF}=\hat{H}_0+\hat{H}'_{MF}$, with $\hat{H}_{MF}=\sum_{\mathbf{k}}\overline{\Psi}^\dagger_{\mathbf{k}}\mathbf{H}_{MF}(\mathbf{k})\overline{\Psi}_{\mathbf{k}}$, $\overline{\Psi}_{\mathbf{k}}=(\Psi_{\mathbf{k}},\Psi_{\mathbf{k}+\mathbf{Q}})^T$, and

$$\mathbf{H}_{MF}(\mathbf{k}) = \begin{bmatrix}\mathbf{H}_0(\mathbf{k}) & \mathbf{H}_1(\mathbf{k},\mathbf{Q})\\ \mathbf{H}_1^\dagger(\mathbf{k},\mathbf{Q}) & \mathbf{H}_0(\mathbf{k}+\mathbf{Q})\end{bmatrix}, \tag{21}$$

$$\mathbf{H_1}(\mathbf{k},\mathbf{Q}) = \begin{bmatrix}0 & iR_{pd}s'_x & iR_{pd}s'_y\\ R_{pd}c'_x & 0 & +R_{pp}c'_xs'_y\\ R_{pd}c'_y & -R_{pp}s'_xc'_y & 0\end{bmatrix}, \tag{22}$$

where $R_{pd}=z_{pd}V_{pd}/t_{pd}$, $R_{pp}=2z_{pp}V_{pp}/t_{pp}$, $s'_x=\sin[(k_x+Q_x)/2]$, $c'_x=\cos[(k_x+Q_x)/2]$, and s'_y,c'_y are

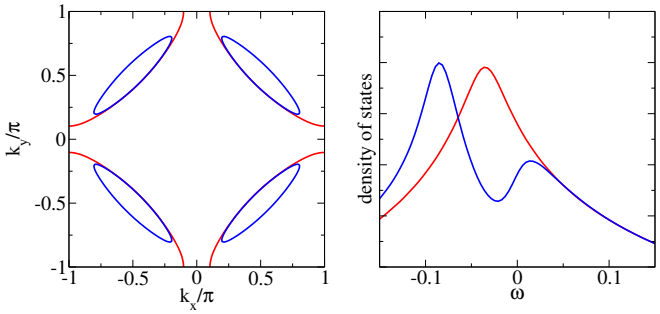

FIG. 5: (Color online) Left: Normal (red) and reconstructed (blue) Fermi surfaces. The loop current strengths are set to $z_{pd} = 0.04$ and $z_{pp} = z_{pd}/3$. The hole density here is $p = 0.10$. Right: Density of states near the Fermi energy.

defined accordingly, and the orbital energies in $\mathbf{H}_0(\mathbf{k})$ are shifted by $\tilde{\epsilon}_d$ and $\tilde{\epsilon}_p$.

We show the reconstructed ($z_{pd} = 0.04$, $z_{pp} = z_{pd}/3$) and normal ($z_{pd} = z_{pp} = 0$) Fermi surfaces and densities of states in Fig. 5. For very small z_{pd} and z_{pp}, hole pockets, as well as small electron pockets near $(\pi, 0)$ and symmetry-related points, are formed. The shapes of the pockets depend on the strength of the loop currents, the hole filling, and the curvature of the unfolded Fermi surface. With increasing z_{pd} and z_{pp}, the electron pockets rapidly disappear, and only the hole pockets persist (Fig. 5). If one takes t_{pd} from band structure calculations, $z_{pd} = 0.04$ corresponds to a p-d current of 16 μA; empirical bandwidths are 3 times smaller,[45] giving a current of 5 μA and a plaquette magnetic moment in the range of $0.05\mu_B$ to $0.09\mu_B$ (see Appendix B).

We propose that the pseudogap appearing at T^* arises from the πLC shown in Fig. 1. Physical properties of staggered currents have been discussed previously[36,41,46,47], and we focus here on aspects related to the recent discoveries of charge order and time-reversal symmetry breaking. The main distinguishing feature of the pseudogap is the depletion of spectral weight along regions of the Fermi surface near $(\pm\pi, 0)$ and $(0, \pm\pi)$.

This leads to a pseudogap in the density of states, as shown in Fig. 5 for the πLC phase. In our calculations z_{pd} is about one third of the peak-to-peak pseudogap; experimental pseudogaps of ~ 100 meV[48] therefore suggest $z_{pd} \sim 0.033$eV, corresponding to a p-d current of $\sim 7\mu A$, consistent with the estimate above.

V. DISCUSSION

Within the phase with staggered loop currents subsequent phase transtions are likely to occur. Notably, we showed previously that persistent discrepancies between theory and experiment regarding the ordering wavevector $\mathbf{q}^*$ of the charge ordered phase are resolved, if the charge order emerges from a preexisting pseudogap phase, rather than causing it. In Ref.[35], a spin-density wave (SDW) with ordering wavevector $\mathbf{Q} = (\pi, \pi)$ was invoked ad hoc as a proxy for the pseudogap in underdoped cuprates. While the presence of a static SDW is not supported by experiment, we view the πLC phase instead as a viable alternative phase out of which a charge-density wave will form with a $\mathbf{q}^*$ that connects adjacent hole pockets. In the coexistence with charge order, the Fermi surface of the πLC phase will further reconstruct. The Fermi surface in the coexistence phase should then serve as the basis to analyze the quantum oscillation experiments which reported evidence for the existence of hole pockets.[49,50]

The πLC phase shares neutron-scattering signatures with the DDW state, specifically an elastic magnetic peak centered at $\mathbf{Q} = (\pi, \pi)$ and the opening of a spin excitation gap. Soon after the original proposal of the DDW state it was argued[51] that the neutron-scattering data obtained by Mook et al. in underdoped YBCO[52] are consistent with the expected features of a DDW state. Other subsequent neutron scattering measurements on oxygen ordered ortho-II YBCO instead[53] reported no evidence for the predicted characteristics of an ordered DDW state. The conflicting results of these experiments have remained unresolved.

An obvious signature of the πLC phase is that it breaks time-reversal symmetry. It does not, however, generate a polar Kerr effect because the pattern in Fig. 1 preserves mirror symmetries. Given this result, an explanation for the observed nonzero Kerr angle at $T_{\rm Kerr}$ requires the onset of a further transition that eliminates these symmetries.[14] This could naturally occur, for example, with the appearance of incommensurate charge order at $T_{\rm co}$. The experimental doping dependences of $T_{\rm Kerr}$[12] and $T_{\rm co}$[54,55] are, however, different; a possible connection between the two is therefore not obvious.

It is nevertheless possible that the different symmetries associated with the charge ordering transition are broken at distinct temperatures.[24] Charge order involves both a continuous broken symmetry associated with the spatial lock-in of the charge modulation, and a discrete broken symmetry associated with the orientation of $\mathbf{q}^*$.[56] In this scenario, $T_{\rm Kerr}$ may signal the onset of a charge-nematic phase, in which only the discrete rotational symmetry is broken, while $T_{\rm co}$ may mark the pinning of the charge modulation by disorder.[56]

We are led to trace the origin of the intriguingly complex physics of underdoped cuprates to the distinct phenomena which emerge from the Coulomb interactions in the CuO_2 planes: the local Coulomb repulsion on the Cu d-orbital is the source of antiferromagnetism in the undoped compounds and of spin-fluctuation mediated d-wave superconductivity upon doping. From the results of this work we conclude that the non-local interaction V_{pd} can cause an orbital current instability, while the non-local interaction V_{pp} is responsible for the charge redistribution between Op_x and Op_y orbitals and incommensurate charge order. V_{pp} and V_{pd} weaken the spin-fluctuation mediated pairing interaction, which suggests a possible reason why $T_c < T_{\rm co}$ below optimal doping.

The physics of underdoped cuprates therefore appears to reflect the mutual competition and/or coexistence of these ordering tendencies.

VI. CONCLUDING REMARKS

Within gRPA, we find no trace of a $\mathbf{q} = 0$ current instability that has been proposed to exist in the three band model. Recently, Weber *et al.* [9] concluded that the charge-transfer energy, $\epsilon_d - \epsilon_p$, is one of the key parameters for this instability. However, over an exhaustive range of this parameter, our calculations did not trace any instability or a sizable enhancement of the $\mathbf{q} = 0$ current susceptibility. Intra-unit cell magnetism has been inferred from spin-flip neutron scattering experiments[3,5]. At this stage, our calculations offer no explanation for this observation.

The close connection between axial charge order with a d-wave form factor[31] and oxygen orbitals makes the three-band model a necessary starting point for the microscopic theory. In this context, the focus has so far been on spin fluctuations, and hence on the local Coulomb interactions U_d and U_p. Our findings, however, point to the important role of non-local interactions. The development of accurate numerical tools capable of handling multi orbital models with intermediate to strong and non-local interactions is, therefore, on demand.

We finally note that, for the typical parameter values used in this work, an SDW phase will, within gRPA, in fact set in at a higher temperature than the πLC phase. This SDW is driven by the local Coulomb interaction U_d on the Cu sites, and it is known that correlation effects beyond the approximations discussed here suppress this SDW. Indeed, the feedback of spin fluctuations renormalizes the electronic structure in a way that reduces the tendency towards antiferromagnetism. We have neglected this aspect here, since we are primarily interested in the charge degree of freedom in the underdoped part of the cuprate phase diagram where pseudogap and charge order occurs. Furthermore, we confirmed that the local interactions U_d and U_p, the key parameters which control antiferromagnetism and spin fluctuations, do not have any effect on the emergence of the πLC phase.

It remains yet to be explored how self-energy corrections in our present approach will influence the instability towards spontaneous loop currents. This is on the agenda for further work on loop currents in the three-orbital model for cuprates.

Acknowledgements

A.P.K. and S.B. were supported by the DFG through TRR80. W.A.A. acknowledges support by the National Sciences and Engineering Research Council (NSERC) of Canada. We thank L. Chioncel for helpful discussions. The calculations were performed on the Linux Cluster of the LRZ in Garching.

[1] A. Shekhter, B. J. Ramshaw, R. Liang, W. N. Hardy, D. A. Bonn, F. F. Balakirev, R. D. McDonald, J. B. Betts, S. C. Riggs, and A. Migliori, Nature (London) **498**, 75 (2013).
[2] B. Fauqué, Y. Sidis, V. Hinkov, S. Pailhès, C. T. Lin, X. Chaud, and P. Bourges, Phys. Rev. Lett. **96**, 197001 (2006).
[3] Y. Li, V. Baledent, N. Barisic, Y. Cho, B. Fauque, Y. Sidis, G. Yu, X. Zhao, P. Bourges, and M. Greven, Nature **455**, 372 (2008).
[4] Y. Li, V. Balédent, N. Barišić, Y. C. Cho, Y. Sidis, G. Yu, X. Zhao, P. Bourges, and M. Greven, Phys. Rev. B **84**, 224508 (2011).
[5] Y. Sidis and P. Bourges, J. Phys.: Conf. Ser. **449**, 012012 (2013).
[6] C. M. Varma, Phys. Rev. B **73**, 155113 (2006).
[7] C. M. Varma, J. Phys.: Condens. Matter **26**, 505701 (2014).
[8] C. Weber, A. Läuchli, F. Mila, and T. Giamarchi, Phys. Rev. Lett. **102**, 017005 (2009).
[9] C. Weber, T. Giamarchi, and C. M. Varma, Phys. Rev. Lett. **112**, 117001 (2014).
[10] R. Thomale and M. Greiter, Phys. Rev. B **77**, 094511 (2008).
[11] Y. F. Kung, C.-C. Chen, B. Moritz, S. Johnston, R. Thomale, and T. P. Devereaux, Phys. Rev. B **90**, 224507 (2014).
[12] J. Xia, E. Schemm, G. Deutscher, S. A. Kivelson, D. A. Bonn, W. N. Hardy, R. Liang, W. Siemons, G. Koster, M. M. Fejer, and A. Kapitulnik, Phys. Rev. Lett. **100**, 127002 (2008).
[13] R.-H. He, M. Hashimoto, H. Karapetyan, J. D. Koralek, J. P. Hinton, J. P. Testaud, V. Nathan, Y. Yoshida, H. Yao, K. Tanaka, W. Meevasana, R. G. Moore, D. H. Lu, S.-K. Mo, M. Ishikado, H. Eisaki, Z. Hussain, T. P. Devereaux, S. A. Kivelson, J. Orenstein, A. Kapitulnik, and Z.-X. Shen, Science **331**, 1579 (2011).
[14] Y. Wang, A. Chubukov, and R. Nandkishore, Phys. Rev. B **90**, 205130 (2014).
[15] T. Wu, H. Mayaffre, S. Krämer, M. Horvatić, C. Berthier, W. N. Hardy, R. Liang, D. A. Bonn, and M.-H. Julien, Nature (London) **477**, 191 (2011).
[16] G. Ghiringhelli, M. Le Tacon, M. Minola, S. Blanco-Canosa, C. Mazzoli, N. B. Brookes, G. M. De Luca, A. Frano, D. G. Hawthorn, F. He, T. Loew, M. M. Sala, D. C. Peets, M. Salluzzo, E. Schierle, R. Sutarto, G. A. Sawatzky, E. Weschke, B. Keimer, and L. Braicovich, Science **337**, 821 (2012).
[17] J. Chang, E. Blackburn, A. T. Holmes, N. B. Christensen, J. Larsen, J. Mesot, R. Liang, D. A. Bonn, W. N. Hardy, A. Watenphul, M. v. Zimmermann, E. M. Forgan, and S. M. Hayden, Nature Phys. **8**, 871 (2012).
[18] E. H. da Silva Neto, P. Aynajian, A. Frano, R. Comin, E. Schierle, E. Weschke, A. Gyenis, J. Wen, J. Schneeloch, Z. Xu, S. Ono, G. Gu, M. Le Tacon, and A. Yazdani,

Science **343**, 393 (2014).
[19] R. Comin, A. Frano, M. M. Yee, Y. Yoshida, H. Eisaki, E. Schierle, E. Weschke, R. Sutarto, F. He, A. Soumyanarayanan, Y. He, M. Le Tacon, I. S. Elfimov, J. E. Hoffman, G. A. Sawatzky, B. Keimer, and A. Damascelli, Science **343**, 390 (2014).
[20] Y. Kohsaka, C. Taylor, K. Fujita, A. Schmidt, C. Lupien, T. Hanaguri, M. Azuma, M. Takano, H. Eisaki, H. Takagi, S. Uchida, and J. C. Davis, Science **315**, 1380 (2007).
[21] W. D. Wise, M. C. Boyer, K. Chatterjee, T. Kondo, T. Takeuchi, H. Ikuta, Y. Wang, and E. W. Hudson, Nat. Phys. **4**, 696 (2008).
[22] M. J. Lawler, K. Fujita, J. Lee, A. R. Schmidt, Y. Kohsaka, C. K. Kim, H. Eisaki, S. Uchida, J. C. Davis, J. P. Sethna, and E.-A. Kim, Nature (London) **466**, 347 (2010).
[23] T. Wu, H. Mayaffre, S. Krämer, M. Horvatić, C. Berthier, W. N. Hardy, R. Liang, D. A. Bonn, and M.-H. Julien, Nat. Commun. **6** (2015).
[24] Y. Wang and A. Chubukov, Phys. Rev. B **90**, 035149 (2014).
[25] P. A. Lee, Phys. Rev. X **4**, 031017 (2014).
[26] D. F. Agterberg, D. S. Melchert, and M. K. Kashyap, Phys. Rev. B **91**, 054502 (2015).
[27] K. B. Efetov, H. Meier, and C. Pépin, Nat. Phys. **9**, 442 (2013).
[28] C. Pépin, V. S. de Carvalho, T. Kloss, and X. Montiel, Phys. Rev. B **90**, 195207 (2014).
[29] D. Chowdhury and S. Sachdev, Phys. Rev. B **90**, 134516 (2014).
[30] L. E. Hayward, D. G. Hawthorn, R. G. Melko, and S. Sachdev, Science **343**, 1336 (2014).
[31] A. J. Achkar, F. He, R. Sutarto, C. McMahon, M. Zwiebler, M. Hucker, G. D. Gu, R. Liang, D. A. Bonn, W. N. Hardy, J. Geck, and D. G. Hawthorn, arXiv:1409.6787 (unpublished).
[32] R. Comin, R. Sutarto, F. He, E. H. da Silva Neto, L. Chauviere, A. Fraño, R. Liang, W. N. Hardy, D. A. Bonn, Y. Yoshida, H. Eisaki, A. J. Achkar, D. G. Hawthorn, B. Keimer, G. A. Sawatzky, and A. Damascelli, Nat. Mater. **14**, 796 (2015).
[33] M. H. Fischer and E.-A. Kim, Phys. Rev. B **84**, 144502 (2011).
[34] S. Bulut, W. A. Atkinson, and A. P. Kampf, Phys. Rev. B **88** (2013).
[35] W. A. Atkinson, A. P. Kampf, and S. Bulut, New J. Phys. **17**, 013025 (2015).
[36] S. Chakravarty, R. B. Laughlin, D. K. Morr, and C. Nayak, Phys. Rev. B **63**, 094503 (2001).
[37] S. Chakravarty, H.-Y. Kee, and K. Völker, Nature (London) **428**, 53 (2004).
[38] V. J. Emery, Phys. Rev. Lett. **58**, 2794 (1987).
[39] M. S. Hybertsen, M. Schlüter, and N. E. Christensen, Phys. Rev. B **39**, 9028 (1989).
[40] P. B. Littlewood, C. M. Varma, S. Schmitt-Rink, and E. Abrahams, Phys. Rev. B **39**, 12371 (1989).
[41] T. C. Hsu, J. B. Marston, and I. Affleck, Phys. Rev. B **43**, 2866 (1991).
[42] D. A. Ivanov, P. A. Lee, and X.-G. Wen, Phys. Rev. Lett. **84**, 3958 (2000).
[43] K. Tsutsui, D. Poilblanc, and S. Capponi, Phys. Rev. B **65**, 020406 (2001).
[44] Y. He, J. Moore, and C. M. Varma, Phys. Rev. B **85**, 155106 (2012).
[45] K. Pasanai and W. A. Atkinson, Phys. Rev. B **81**, 134501 (2010).
[46] R. B. Laughlin, Phys. Rev. B **89**, 035134 (2014).
[47] I. Dimov, P. Goswami, X. Jia, and S. Chakravarty, Phys. Rev. B **78**, 134529 (2008).
[48] T. Kurosawa, T. Yoneyama, Y. Takano, M. Hagiwara, R. Inoue, N. Hagiwara, K. Kurusu, K. Takeyama, N. Momono, M. Oda, and M. Ido, Phys. Rev. B **81**, 094519 (2010).
[49] N. Doiron-Leyraud, C. Proust, D. LeBoeuf, J. Levallois, J.-B. Bonnemaison, R. Liang, D. A. Bonn, W. N. Hardy, and L. Taillefer, Nature (London) **447**, 565 (2007).
[50] S. E. Sebastian, N. Harrison, and G. Lonzarich, Rep. Prog. Phys. **75**, 102501 (2012).
[51] S. Chakravarty, H.-Y. Kee, and C. Nayak, Int. J. Mod. Phys. B **15**, 2901 (2001).
[52] H. A. Mook, P. Dai, and F. Dogan, Phys. Rev. B **64**, 012502 (2001).
[53] C. Stock, W. J. L. Buyers, Z. Tun, R. Liang, D. Peets, D. Bonn, W. N. Hardy, and L. Taillefer, Phys. Rev. B **66**, 024505 (2002).
[54] M. Hücker, N. B. Christensen, A. T. Holmes, E. Blackburn, E. M. Forgan, R. Liang, D. A. Bonn, W. N. Hardy, O. Gutowski, M. v. Zimmermann, S. M. Hayden, and J. Chang, Phys. Rev. B **90**, 054514 (2014).
[55] S. Blanco-Canosa, A. Frano, E. Schierle, J. Porras, T. Loew, M. Minola, M. Bluschke, E. Weschke, B. Keimer, and M. Le Tacon, Phys. Rev. B **90**, 054513 (2014).
[56] L. Nie, G. Tarjus, and S. A. Kivelson, Proc. Nat. Acad. Sci. **111**, 7980 (2014).

Appendix A: Current operators

The current operator is conventionally defined as

$$\hat{J}_{ij} = -it_{ij}(\hat{c}_i^\dagger \hat{c}_j - \hat{c}_j^\dagger \hat{c}_i). \tag{A1}$$

At this point, however, it is important to take into account that we are working with a Hamiltonian which is gauge transformed according to Equations (6)-(9). In the transformed operator basis, the current operators in real space take the following form:

$$J_{id,jx} = t_{id,jx}(\hat{c}_{id}^\dagger \hat{c}_{jx} + \hat{c}_{jx}^\dagger \hat{c}_{id}) \tag{A2}$$

$$J_{ix,jd} = -t_{ix,jd}(\hat{c}_{id}^\dagger \hat{c}_{jx} + \hat{c}_{jx}^\dagger \hat{c}_{id}) \tag{A3}$$

$$J_{id,jy} = t_{id,jy}(\hat{c}_{id}^\dagger \hat{c}_{jy} + \hat{c}_{jy}^\dagger \hat{c}_{id}) \tag{A4}$$

$$J_{iy,jd} = -t_{iy,jd}(\hat{c}_{id}^\dagger \hat{c}_{jy} + \hat{c}_{jy}^\dagger \hat{c}_{id}) \tag{A5}$$

$$J_{ix,jy} = -it_{ix,jy}(\hat{c}_{ix}^\dagger \hat{c}_{jy} - \hat{c}_{jy}^\dagger \hat{c}_{ix}) \tag{A6}$$

$$J_{iy,jx} = -it_{iy,jx}(\hat{c}_{iy}^\dagger \hat{c}_{jx} - \hat{c}_{jx}^\dagger \hat{c}_{iy}). \tag{A7}$$

Appendix B: Estimating the resulting magnetic moment

Here, we perform a simple estimate of the magnetic moment associated with the πLC loop currents.

We start by expressing the currents in absolute units. The unit of the current operators is $e[t_{ij}]/[\hbar] =$

$C(eV)/(eV \cdot s) = C/s$. For $z_{pd} = 0.04t_{pd}$, the current along p-d bonds is $I_{pd} = z_{pd} \times (e/\hbar) = 0.04t_{pd} \times (2.4 \times 10^{-4})A = 9.6t_{pd}\mu A$, where t_{pd} is measured in eV. Band structure calculations suggest $t_{pd} \approx 1.6$ eV, yielding $I_{pd} = 16$ μA; experimental bandwidths, however, are typically a factor of 3 smaller than predicted by band structure calculations suggesting $I_{pd} \sim 5$ μA. This is comparable to other estimates of loop current amplitudes: within a cluster calculation of multi-orbital t-J model, the upper bound of θ_{II}-like loop currents was previously estimated to be between $5\mu A$ and $15\mu A$ for different parameter sets[10]; similarly, in the single band DDW studies, the staggered loop currents were estimated to be $\sim 7\mu A$ by assuming a DDW gap value of ~ 0.03eV[36].

Next, we calculate the magnetic moments of loop currents using the formula $M = I\eta$ where I is the current, and η is the area enclosed by the loop. This is indeed a crude calculation, however we believe this should yield a qualitatively correct number. The total magnetic moment in a given plaquette has two contrubutions: $I_b\eta_b$ and $I_g\eta_g$ due to two independent current loops (shown in black and green in Fig. 1). We set $I_b = 5\mu A$, and since it circulates around the whole plaquette, $\eta_b = a^2$. As given by the eigenvectors of $\chi^J(q)$, $I_g \approx I_{pd}/3$, and it circulates around an area of $\eta_g = a^2/2$. Thus, the magnetic moment is calculated as

$$\begin{aligned} M &= I_b\eta_b + I_g\eta_g && \text{(B1)} \\ &= I_{pd} \times a^2 + I_{pd}/3 \times a^2/2 && \text{(B2)} \\ &= 7I_{pd}a^2/6 && \text{(B3)} \\ &= 7(5\mu A)(3.85 \times 10^{-10}m)^2/6 && \text{(B4)} \\ &\approx 0.09\mu_B. && \text{(B5)} \end{aligned}$$

However, since I_{pd} is shared by the neighbouring plaquettes, the effective moment for individual plaquettes might be reduced to $\sim 0.05\mu_B$.